Structural Basis for Interaction of FGF-1, FGF-2, and FGF-7 with Different Heparan Sulfate Motifs[†,‡]

Sheng Ye,[§,||,⊥] Yongde Luo,[||,#] Weiqin Lu,[#,▽] Richard B. Jones,[#,○,×] Robert J. Linhardt,[◇] Ishan Capila,[◇] Toshihiko Toida,[■] Mikio Kan,[#,▲] Huguette Pelletier,[§] and Wallace L. McKeehan[*,#,○]

Department of Biochemistry, Baylor College of Medicine, One Baylor Plaza, Houston, Texas, 77030, Department of Biochemistry and Biophysics, Texas A&M University and Center for Cancer Biology and Nutrition, Institute of Biosciences and Technology, Texas A&M University System Health Science Center, Houston, Texas, 77030-3303, Division of Medicinal and Natural Products Chemistry, Department of Chemistry, and Department of Chemical and Biochemical Engineering, University of Iowa, Iowa City, Iowa, 52240 and Faculty of Pharmaceutical Sciences, Chiba University, 1-33 Yayoi-cho, Inage-ku, Chiba-city, Chiba 263-8522, Japan

Received May 16, 2001; Revised Manuscript Received August 8, 2001

ABSTRACT: Stromal cell-derived FGF-7 binds and activates only the resident FGFR2IIIb in epithelial cells while FGF-1 and FGF-2 exhibit a broader interaction with multiple isoforms of FGFR. Here we report the structure of FGF-7 that has been solved to 3.1 Å resolution by molecular replacement with the structure of a dual function chimera of FGF-7 and FGF-1 (FGF-7/1) which was resolved to 2.3 Å. Comparison of the FGF-7 structure to that of FGF-1 and FGF-2 revealed the strongly conserved Cα backbone among the three FGF polypeptides and the surface hydrophobic patch that forms the primary receptor-binding domain. In contrast, a decrease and dispersion of the positive surface charge density characterized the heparin-binding domain of FGF-7 defined by homology to that of FGF-1 and FGF-2 in complexes with heparin. A simple heparin hexasaccharide that cocrystallized with FGF-1 and FGF-2 and protected both against protease in solution failed to exhibit the same properties with FGF-7. In contrast to FGF-1 and FGF-2, protection of FGF-7 was enhanced by heparin oligosaccharides of increased length with those exhibiting a 3-O-sulfate being the most effective. Protection of FGF-7 required interaction with specifically the fraction of crude heparin retained on antithrombin affinity columns. Conversely, heparin enriched by affinity for immobilized FGF-7 exhibited anti-factor Xa activity similar to that purified on an antithrombin affinity matrix. In contrast, an FGF-1 affinity matrix enriched the fraction of crude heparin with low anti-factor Xa activity. The results provide a structural basis to suggest that the unique FGF-7 heparin-binding (HB) domain underlies a specific restriction in respect to composition and length of the heparan sulfate motif that may impact specificity of localization, stability, and trafficking of FGF-7 in the microenvironment, and formation and activation of the FGFR2IIIb kinase signaling complex in epithelial cells.

The fibroblast growth factor (FGF)[1] signal transduction system is ubiquitous and a mediator of developmental processes in the embryo and homeostasis in the adult (*1*, *2*). The family in mammals is currently comprised of 23 FGF homologues and four transmembrane tyrosine kinase receptors (FGFR). The latter exhibit extensive diversity of structure and function through combinatorial splicing (*2*). Through intimate associations of both FGF and the FGFR ectodomain with heparan sulfate chains of the peri-cellular matrix or transmembrane proteoglycans, the FGFR signaling complex is controlled by and is responsive to perturbation and remodeling of the peri-cellular microenvironment. Heparan sulfate has been implicated in stability of FGF (*3*), sequestration and access of FGF to the FGFR complex (*4*−*6*), oligomerization of FGF (*7*−*11*) and FGF−FGFR complexes

† This work was supported by NIH Grants DK35310, DK47039, and CA59971 to W.L.M. and GM38060 and HL52622 to R.L.

‡ Coordinates have been deposited in the RCSB Protein Data Bank: code 1QQK for FGF7 and 1QQL for FGF7/1.

* To whom correspondence should be addressed. Phone: (713) 677-7522. Fax: (713) 677-7512. E-mail: wmckeeha@ibt.tamu.edu.

§ Department of Biochemistry.

|| Contributed equally to the work.

⊥ Current address: Department of Biochemistry, University of Texas Southwestern Medical Center at Dallas, 5323 Harry Hines Blvd., Dallas, TX 75390.

Center for Cancer Biology and Nutrition.

▽ Current address: Department of Molecular & Human Genetics, Baylor College of Medicine, One Baylor Plaza, Houston, TX 77030.

○ Department of Biochemistry and Biophysics.

× Current address: Department of Molecular and Cellular Biology, Harvard University, 16 Divinity Ave., Cambridge, MA 02138.

◇ Division of Medicinal and Natural Products Chemistry.

■ Faculty of Pharmaceutical Sciences.

▲ Current address: Central Research Laboratories, Zeria Pharmaceutical Co., Ltd., 2512-1 Oshikiri, Kohnan-machi, Ohsato-Gun, Saitama, 360-0111, Japan.

[1] Abbreviations: FGF, fibroblast growth factor; FGFR, FGF receptor kinase; H-patch, surface hydrophobic patch; HB domain, heparin-binding domain; Se-Met, seleno-methionyl; MAD, multiwavelength anomalous diffraction; GST, glutathione-S-transferase; FPLC, fast performance liquid chromatograph; ATIII, antithrombin III; MIR, multiple isomorphous replacement; rmsd, root-mean-square deviation; Ig, immunoglobulin; G-box, glycine-box; GlcA, D-glucuronic acid; GlcN, D-glucosamine; GlcNS, *N*-sulfo-D-glucosamine; IdoA, L-iduronic acid; GSH, reduced glutathione; Con A, concanavalin A; 1QQL, RCSB Protein Data Bank code for chimera FGF-7/1; 1QQK, Protein Data Bank code for FGF-7.

10.1021/bi011000u CCC: $20.00 © 2001 American Chemical Society
Published on Web 11/06/2001

(*2*, *9*, *12*), and conformational repression and activation of FGFR oligomers (*2*, *13*).

FGF-7 (also called KGF for keratinocyte growth factor) is distinguished as a directional mediator of mesenchymal cell instructions to epithelial cells (*14*−*16*). It is expressed in the mesenchymal cells of parenchymal organs and signals by activation of a splice variant of the FGFR2 gene (FGFR2IIIb) that is exclusively expressed in epithelial cells (*14*−*16*). Loss of responsiveness to stromal FGF-7 correlates with progression to malignancy in model prostate tumors (*15*, *16*). These properties and its broad importance as a mediator of mesenchymal-epithelial communication provide a strong rationale to understand the structural basis of FGF-7 signaling. Among the 23 mammalian FGF homologues and homologues from other species, the structures of only mammalian FGF-1 (also called acidic FGF) and FGF-2 (also called basic FGF), which have a much broader reactivity for FGFR isotypes, are available for comparison (*11*, *17*−*19*). We determined the structure to 2.3 Å of a dual function chimera of FGF-7 and the C-terminus of FGF-1, which gained ability to bind the FGFR2IIIc variant without significant loss of binding to FGFR2IIIb, and used it to resolve the structure of FGFR2IIIb-specific FGF-7 to 3.1 Å (*20*). A comparison of the structure of FGF-7 with those of FGF-1 and FGF-2 revealed a highly conserved Cα backbone and surface hydrophobic patch (H-patch) that comprises a common primary receptor interaction domain among the three homologues. On the basis of the homology of the heparin-binding domain (HB domain) of FGF-1 and FGF-2 in crystal complexes with a heparin oligosaccharide, the FGF-7 structure revealed a unique HB domain that, in contrast to FGF-1 and FGF-2, interacted only with heparin exhibiting anti-Factor Xa and antithrombin-binding activity. Both results of the structural and functional interaction analysis in solution suggest a unique FGF-7 HB domain that requires a specific heparan sulfate motif that has some overlapping structural features with anticoagulant heparin. This may underlie specific localization, stability, and trafficking of FGF-7 in the microenvironment. In addition, the unique HB domain may pose added restrictions on composition and length of the heparan sulfate chain required to participate in formation and activation of the FGFR2IIIb kinase signaling complex in epithelial cells.

EXPERIMENTAL PROCEDURES

Expression, Purification, and Crystallization of FGF-7 and the Chimera FGF-7/1. Procedures for expression and purification of recombinant rat FGF-7 and FGF-7/1 (rat FGF-7/human FGF-1, mutant FGF-7m1) in bacteria have been described (*20*). The seleno-methionyl (Se-Met) FGF-7 and FGF-7/1 chimera was expressed in methionine auxotroph *Escherichia coli* B834 (DE3) (*21*).

Two different crystal forms of FGF-7 were obtained at room temperature using sitting drop vapor diffusion with FGF-7 at 10 mg/mL in 10 mM Hepes (pH 7.0). FGF-7 was concentrated and exchanged into buffers using a Centricon-10 (Amicon). Monoclinic crystals were grown over reservoir solutions containing 18.5% PEG 3350, 50 mM NaCl, and 0.1 M citrate (pH 4.7). They belonged to the space group $P2_1$ with $a = 61.1$ Å, $b = 35.5$ Å, $c = 115.3$ Å, $\beta = 101.0°$ when frozen and contained about 40% solvent with four molecules in the asymmetric unit. Glycerol was employed as a cryoprotectant here and in subsequent experiments. The yield and stability of monoclinic crystals, which appeared to have four molecules of FGF-7 per asymmetric unit, was a major difficulty. Crystals were prone to deteriorate during growth and turned mosaic after 2−3 weeks requiring prompt diffraction analysis prior to that period. Tetragonal crystals of FGF-7 also emerged over reservoir solutions containing 2.56 M sodium/potassium phosphate (pH 5.0) and 0.1 M sodium citrate. They belonged to the space group $I4_122$ with $a = 169.1$ Å, $c = 62.6$ Å when frozen and contained about 67% solvent with two molecules in the asymmetric unit. Seeding was essential in growing diffracting crystals of both forms from FGF-7. The monoclinic crystal forms of FGF-7 diffracted at 4.5 Å and the tetragonal form to 3.8 Å using normal monochromatized CuKα radiation generated from a Rigaku RU200 rotating-anode X-ray generator. These conditions also yielded crystals of Se-Met FGF-7.

The purified Se-Met chimera FGF-7/1 was concentrated to 10 mg/mL and exchanged into 10 mM Hepes (pH 7.0), 20 mM $(NH_4)_2SO_4$, 10 mM DTT and 0.2 mM EDTA using a Centricon-10 (Amicon). Crystals were grown at 20 °C by vapor diffusion in sitting drops containing equal volumes of protein solution and the reservoir solution (1.75 M sodium/potassium phosphate, pH 7.0, 20 mM DTT). The resulting crystals belonged to the hexagonal space group $P6_422$ with unit cell dimensions of $a = 89.8$ Å and $c = 65.5$ Å when frozen. There was one FGF-7/1 molecule in the asymmetric unit with solvent content of 57%.

Data Collection, Structure Determination, and Refinement. Data were collected with ADSC Quantum-4 CCD detectors at CHESS and with MAR image plate detector at SSRL. Native tetragonal FGF-7 crystals diffracted to 3.1 Å on beamline F-1 at CHESS, and a set of data was collected. The monoclinic crystals of FGF-7 diffracted to 3.3 Å on beamline 7-2 at SSRL, and a native data set was also collected. The tetragonal crystals of Se-Met FGF-7 diffracted poorly on beamline F-2 at CHESS. After the failure of attempts at MAD phasing, the approach was abandoned. The crystals of the Se-Met FGF-7/1 chimera diffracted to 2.3 Å on beamline F-2 at CHESS. Multiwavelength anomalous diffraction (MAD) data sets were collected at three wavelengths near the Se absorption edge using the inverse beam mode. All data were processed using DENZO and SCALEPACK (*22*).

The MAD data for the FGF-7/1 chimera was phased by treatment of one of the wavelengths ($\lambda 3$) as the "native" or reference. The other wavelengths were treated as the "derivative" (*23*) using a Bayesian approach. The three wavelengths were reduced to single isomorphous and anomalous scattering contributions (*24*). The program SOLVE (see http://www.solve.lanl.gov/) was used to automatically reduce the integrated, scaled intensities to structure factors, perform local scaling with respect to the reference wavelength, solve for the heavy-atom positions, and refine heavy-atom phases. The phases produced by SOLVE were used to calculate an electron density map using the CCP4 package and solvent flattened using the program DM assuming a solvent content of 57%. The final solvent-flattened map was of excellent quality. An initial model for 131 of the 140 protein residues of FGF-7/1 could be built into the solvent-flattened map

Table 1: Crystallographic Analysis

Diffraction Data

data set	wavelength (Å)	resolution (Å)	reflections	redundancy	completeness (%)	R_{sym} (%)[d]
FGF-7 ($I4_122$)[a]	0.9296	30−3.1	8036 (48 247)[b]	6.0	94.2 (81.6)[c]	12.9 (44.7)[c]
FGF-7 ($P2_1$)[a]	1.08	30−3.3	6389 (19 413)[b]	3.0	83.4 (65.6)[c]	6.2 (48.1)[c]
Se-Met FGF-7/1 ($P6_422$)[a]	0.9794	30−2.3	7151 (62 741)[b]	8.9	96.5 (92.9)[c]	6.6 (31.6)[c]
	0.9792	30−2.3	7150 (62 706)[b]	8.9	96.9 (96.0)[c]	6.3 (30.7)[c]
	0.9639	30−2.3	7140 (64 157)[b]	9.0	96.8 (95.0)[c]	6.5 (29.9)[c]

Model Refinement[e]

refinement	resolution (Å)	*R*-value (%)[f]	rms bond distance (Å)	rms angles (deg)	non-H atoms	Ramachandran plot residues in generally allowed regions (%)
FGF-7 ($I4_122$)[a]	10−3.1	23.3 (32.4)[g]	0.015	2.13	2157 (128)[h]	3.5
Se-Met FGF-7/1 ($P6_422$)[a]	6−2.3	23.7 (32.8)[g]	0.016	2.10	1242 (159)[h]	2.6

[a] Space group. [b] Total number of measurements. [c] Highest resolution shell. [d] $R_{sym} = 100 \times \sum_{hkl}\sum_i|I_i - \langle I\rangle|/\sum_{hkl}\sum_i I_i$, where I_i is the ith measurement; $\langle I\rangle$ is the weighted mean of all measurements of I, and h, k, l are the reflection indices. [e] Statistics for data with $F > 2\sigma$. [f] *R*-value $= 100 \times \sum||F_o| - |F_c||/\sum|F_o|$, where F_o are the observed structure factors and F_c are the calculated structure factors. [g] Free *R*-value. [h] Number of water molecules.

using the program O (*25*). Identification and initial fitting of segments of the amino acid sequence were facilitated by the location of the seleno-methionines. For refinement of the protein, the 2.3 Å data of the remote wavelength were used. The model was subjected to several cycles of molecular dynamics and restrained refinement with X-PLOR (*26*) and manual rebuilding. The refinement statistics are shown in Table 1. The first eight N-terminal residues and the C-terminal residue were disordered. The raw diffraction data and coordinates of the refined model have been deposited in the RCSB Protein Data Bank (PDB code 1QQL).

Since MAD phasing failed with the Se-Met form of FGF-7, the FGF-7 structure in the tetragonal crystal form was determined by molecular replacement using AMoRe (*27*). The solution of the cross-rotation function (20.0−4.0 Å) using the structure of 72% identical FGF-7/1 with nonconserved side chains truncated to alanine as a search model was initially noisy without an obvious peak. However, the translation function yielded a solution for the first molecule (correlation coefficient 33.5%; *R*-factor of 48.3%) from the second peak of the cross-rotation function. The second molecule was found in a partial translation function with the first molecule fixed (correlation coefficient 45.0%; *R*-factor of 44.5%) from the sixth peak of the cross-rotation function. Further refinement was done, and maps were calculated using X-PLOR (*26*). Maps were viewed with program O (*25*). Due to poor side-chain density, Asp-9, Lys-32, Glu-60 of molecule A, and Lys-32, Gln-35, Glu-36, Glu-62, Lys-77, Glu-78, Leu-88, Lys-116, Arg-121, Lys-126 of molecule B were modeled as alanine. There are two looped regions, residues 91−93 and 100−110, with large differences in rmsd between molecules in the asymmetric unit. The first eight N-terminal residues of the two molecules, residues 103−105 of molecule A, residues 79−81, residues 106−108, and the C-terminal residue of molecule B, all located in loops at the protein surface, had insufficient density and were not modeled. Molecule A was chosen for further structural analysis. The raw data and coordinates of the model have been deposited in the Protein Data Bank (PDB code 1QQK).

The monoclinic form of FGF-7 crystal that diffracted at 3.3 Å resolution had a predicted four molecules per asymmetric unit, diffracted with low completeness (83.4%) and low redundancy (3.0) and yielded weak signals in the rotation and translation functions. Attempts at molecular replacement failed to extract signal from noise and the crystal form was not considered further.

Attempts to resolve the structure of FGF-7 from data sets collected at SSRL with FGF-1 and FGF-2 as the search model despite the 30% sequence identity failed. This was limited by the small size of the FGFs that caused a noisy rotation function due to multiplicity of intermolecular vectors in the Patterson Function independent of integration volume combined with the insufficient resolution and insufficient homology. The predicted four molecules per asymmetric unit in one crystal form compounded the difficulty. A native data set with resolution to 2.8 Å was obtained with a conventional detector from the $P6_422$ form of the FGF-7/1 chimera, which shares 60% sequence identity with FGF-1. However, attempts at solution of the structure by molecular replacement with the FGF-1 model failed, despite the space group containing one molecule in the asymmetric unit, the higher resolution, and higher sequence homology. The high degree of internal symmetry in the structures of the FGF family of polypeptides may also underlie difficulties in the molecular replacement approach. The structure of the FGF-7/1 chimera, which shares 72% sequence identity with FGF-7, provided the bridge that solved the FGF-7 structure by molecular replacement. To date, we have been unable to phase the FGF-7 data from the monoclinic crystal form by molecular replacement, even with the refined FGF-7 structure from the tetragonal crystal form. Attempts with dimeric models of the FGF-7 structure were also unsuccessful. This appears to be due to the internal pseudo-symmetry of the molecule, which interferes with the rotation function.

Interaction of Heparin and Oligosaccharides with FGF. The heparin hexasaccharide that does not bind to antithrombin and exhibits no anti-factor Xa activity was the same as that which cocrystallized with FGF-2 (*19*). The antithrombin-

binding decasaccharide (10-mer, AT10) was prepared, purified to homogeneity, and characterized as previously described (*28*). It has the structure ΔUAp2S(1→4)-α-D-GlcNpS6S(1→4)-α-L-IdoAp2S(1→4)-α-D-GlcNpS6S−(1→4)-α-L-IdoAp2S(1→4)-α-D-GlcNpS6S−(1→4)-α-L-IdoAp(1→4)-α-D-GlcNpAc6S(1→4)-β-D-GlcAp(1→4)-α-D-GlcNpS3S6S (*29*, *30*). The AT10 decasaccharide exhibited a partial antithrombin-III-binding site with the α-D-GlcNpS3S6 at the reducing terminus. AT10 exhibited a K_d for ATIII that was 80 times that of full-length heparin (mean molecular mass 13 000 Da), an IC_{50} for inhibition of factor Xa that was 1.8 times that of low molecular weight heparin (5000−8000), and no anti-factor IIa activity (*30*). The antithrombin-binding tetradecasaccharide (14-mer, AT14) was prepared in >90% purity and characterized by multidimensional NMR spectroscopy (*28*). While the saccharide composition and the presence of a α-D-GlcNpS3S6S residue could be confirmed, the precise placement within the tetradecasaccharide is still unclear although it is suspected to be at the reducing terminus similar to that of AT10. The tetradecasaccharide exhibited an anti-factor Xa activity equivalent to AT10. Complete characterization is in process. The heparin decasaccharide and tetradecasaccharide that do not bind to antithrombin have the structure of ΔUAp2S(1→4)[-α-D-GlcNpS6S(1→4)-α-L-IdoAp2S(1→4)]$_4$-α-GlcNpS6S and ΔUAp2S(1→4)[-α-D-GlcNpS6S(1→4)-α-L-IdoAp2S(1→4)]$_6$-α-GlcNpS6S, respectively.

Crude porcine intestinal mucosal heparin (product number H3393, 179 USP units/mg, Sigma, St. Louis, MO) was fractionated by antithrombin affinity chromatography (*31*). Protease protection assays (*3*) were performed with 2 ng of the indicated [^{125}I]FGF (1−4 × 10^5 cpm/ng), 15 ng, 75 ng, and 150 ng of Pronase (Roche Molecular Biochemicals, Indianapolis, IN) for FGF-1, FGF-2, and FGF-7, respectively. Assays contained the indicated amounts of heparin or heparin-derived oligosaccharide in 100 μL of PBS containing 10 mM magnesium chloride and 1% Triton X-100. After incubation overnight at 37 °C, analysis on 15% SDS−PAGE plus autoradiography or precipitation with trichloroacetic acid (TCA) was employed to quantify the remaining FGF that was resistant to protease. As reported previously (*20*), heparin protects the active core of FGFs against degradation by trypsin and other proteases (unpublished results). Pronase and the indicated concentrations of it were chosen for this series of experiments after screening for conditions (type of protease, concentration of protease, time, and temperature) which yielded the highest signal-to-noise ratio (plus crude heparin/minus crude heparin) for each FGF isotype. Under these conditions, over 90% of the protected radiolabeled products of the three FGFs assessed by TCA precipitation was present in a single band with apparent molecular weight identical to the starting product. No additional lower molecular weight bands could be detected by prolonged exposure of gels. FGF-1 and FGF-7 were expressed as recombinant fusion proteins with GST fused on the N-terminus at alanine-1 and alanine-30, respectively (*20*). Homogeneous ^{15}Phe-FGF-1 (apparent molecular mass 16.5 kDa) and ^{154}Ser-FGF-7 (apparent mass 17 kDa) were generated by treatment with trypsin while immobilized on heparin-Sepharose and then purified by reversed-phase HPLC and radiolabeled as described (*20*). Recombinant bacterial FGF-2 (apparent mass 17.5 kDa) was purchased from Upstate Biotechnology, Inc. (Lake Placid, NY). Apparent molecular mass was estimated on 15% SDS−PAGE.

Inhibition of Factor Xa Activity by FGF-7 Affinity-Purified Heparin. Rat FGF-7 and human FGF-1 fused to glutathione-S-transferase (GST) (*20*) were purified first on heparin-Sepharose (Amersham Pharmacia Biotech, Alameda, CA). The factors were then immobilized on GSH-Sepharose (Amersham Pharmacia Biotech, Alameda, CA), washed with 1 M NaCl in elution buffer (10 mM Tris-HCl, pH 7.4, and 1 mM DTT), and utilized as an affinity matrix for fractionation of crude heparin.

Porcine intestinal mucosal heparin (10 mg) was loaded on a 2 mL column of GSH-Sepharose, which contained 20 mg of bound GST-FGF and then eluted stepwise with 0.3, 0.6, 0.9, and 1.3 M NaCl in 10 mM Tris-HCl (pH 7.4) and 1 mM DTT. Heparin was detected by absorbance at 226 nm using a fast performance liquid chromatograph (FPLC) (Amersham Pharmacia Biotech, Alameda CA). The fraction that eluted at 0.3 M NaCl was defined as the "unbound" fraction and repeatedly applied to a fresh column and eluted in order to ensure complete removal of the fraction of heparin denoted as "bound." A negligible amount of heparin eluted at 1.3 M NaCl from the GST-FGF-7 matrix and was not considered further while the 0.6, 0.9, and 1.3 M NaCl fractions from the GST-FGF-1 column were evaluated. Each fraction was dialyzed against water and freeze-dried, and the content of heparin was determined by the carbazole assay.

Antithrombin III (ATIII) was purified from human plasma obtained from The Blood Center (Houston, TX) by affinity chromatography on a heparin-Sepharose column. The clarified blood was absorbed on the column at 0.7 M NaCl in 10 mM Tris-HCl (pH 7.4) containing 1 mM $CaCl_2$, 1 mM $MgCl_2$, and 1 mM $MnCl_2$ followed by extensive washing with the same solution. About 15−20 mg of ATIII/L of plasma was recovered by elution with 2.0 M NaCl in the same buffer. About 10 mg of purified ATIII was loaded onto a 2 mL column of concanavalin A (Con A)-Sepharose (Amersham Pharmacia Biotech, Alameda, CA) and equilibrated with the above buffer containing 0.15 M NaCl. The column was washed sequentially with the same buffer containing 0.5 M NaCl, 1.0 M NaCl, and then 0.15 M NaCl, and then used for fractionation of heparin. The eluate at 0.3 M NaCl and that between 0.3 and 2.0 M NaCl was designated as the unbound and bound fractions, respectively.

For the assay of factor Xa activity, 10 μL fractions containing 1 μg/mL heparin were mixed with 10 μL of 1.7 μM ATIII purified as described above. The mixture was incubated at 37 °C for 2 min, and then 70 μL of 10 nM factor Xa (New England BioLabs, Beverly, MA) was added. After 5 min at 37 °C, 10 μL of 4 mM Chromozym X (Roche Molecular Biochemicals, Indianapolis, IN) was added. The reaction was stopped by addition of 10 μL of glacial acetic acid. The remaining Factor Xa activity was recorded for 5 s at 405 nm in a 96-well plate reader (Molecular Devices Corp. Menlo Park, CA).

RESULTS AND DISCUSSION

Protein Preparation and Crystallization. By application of a novel production and recovery procedure (*20*, *32*), we obtained a yield of FGF-7 crystals in monoclinic and

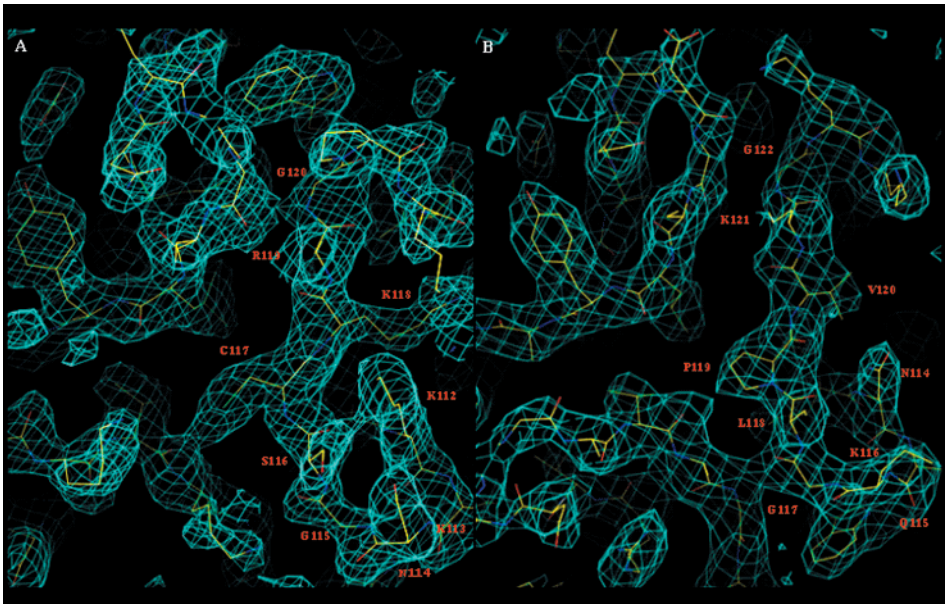

FIGURE 1: Stereo representation of electron density maps. (A) The electron density in the region of the glycine-box at 1.2σ calculated to 2.3 Å with the model phase of FGF-7/1. Superimposed on the density is the final refined model of FGF-7/1. (B) The electron density map in the same region at 1.2σ calculated to 3.1 Å with the model phase of FGF-7. Superimposed on the density is the final refined model of FGF-7.

tetragonal form that diffracted to 3.3 and 3.1 Å, respectively. Attempts to determine phase by a combination of molecular replacement with the available FGF-1 and FGF-2 structures, multiple isomorphous replacement (MIR), and multiwavelength anomalous diffraction (MAD) failed (Experimental Procedures). As an alternative approach, we determined the structure of a dual function chimera (FGF-7/1) constructed from exons 1 and 2 from rat FGF-7 and exon 3 from human FGF-1 (*20*) as a potential phasing model with higher homology to FGF-7.

Structures of the FGF-7/1 Chimera and FGF-7. The crystal structure of chimeric FGF-7/1 was determined by multiwavelength anomalous diffraction and was refined at 2.3 Å resolution to an *R*-factor and an R_{free} of 23.7 and 32.8% (Table 1). The statistics of intensity ratio ($\langle|I|^2\rangle/\langle|I|\rangle^2$) and Wilson ratio ($\langle|F|\rangle^2/\langle|F|^2\rangle$) for FGF-7/1 was 2.08 and 0.781, which strongly suggested that the FGF-7/1 crystal was a single crystal eliminating the possibility that partial merohedral twinning contributed to the data. We were unable to further reduce the notably high R_{free} by repeated analysis and refinement using X-PLOR. However, the well-defined electron density map matched the model perfectly (Figure 1). The model from the structure of the FGF-7/1 chimera was then employed to resolve the three-dimensional structure of FGF-7 in the tetragonal crystal form by molecular replacement and has been refined at 3.1 Å resolution to an *R*-factor and an R_{free} of 23.3 and 32.4%, respectively (Table 1). The two independent FGF-7 molecules within the asymmetric unit are similar and can be overlapped with a root-mean-square deviation (rmsd) of about 1.01 Å between α carbons, and their electron density is well-defined (Figure 1). This exceeded the 0.26−0.87 Å rmsd among different molecules reported for FGF-1 (*11*, *17*) and the 0.57 Å for FGF-2 (*17*). Two looped regions (loop 91−93, 100−110) with relatively large differences (4.4 Å for residue 92 and 4.3 Å for residue 101) in the two molecules contributed significantly to the larger rmsd. In loop 91−93, a hydrogen bond (3.2 Å) formed between Asn-92 Oδ1 of molecule B and the backbone N of Arg-38 of symmetry related molecule B. Another hydrogen bond (3.2 Å) formed between His-93 Nϵ2 of molecule B and the carbonyl O of Gln-35 of symmetry related molecule B. These two hydrogen bonds were not observed in molecule A, suggesting that the large difference is caused by packing. The disorder in residues 103−105 in, specifically, molecule A and residues 106−108 in, specifically, molecule B suggests that loop 100−110 is a very flexible surface loop in FGF-7. The 1.01 Å rmsd for FGF-7 together with the overall difficulties in obtaining quality crystals, the observed stability of crystals, and generally low diffraction resolution suggests that the structure of FGF-7 in absence of heparin/heparan sulfate may be intrinsically more flexible than that of FGF-1 and FGF-2.

Although there was only one molecule in an asymmetric unit for the FGF-7/1 chimera, there were two molecules in the unit for the productive tetragonal crystal form of FGF-7. The side chains of three residues in molecule A and 10 residues in molecule B of FGF-7 were disordered. Molecule A was chosen for modeling and calculation of the surface potential for FGF-7. The first eight N-terminal residues of both the FGF-7/1 chimera and FGF-7 were disordered. The 12 β strands characteristic of FGFs were arranged into 10 well-defined and two poorly defined antiparallel strands in a pattern with approximate 3-fold internal symmetry (Figure 2). The first β-strand in FGF-7 and FGF-7/1 chimera was three amino acids longer than that of FGF-1 and FGF-2. β-Strands 6 and 7 of FGF-7 and the last β-strand of the FGF-7/1 chimera were only three residues long, the shortest among the four structures. Cys-17 is completely buried and Cys-83 is near the surface. Both are conserved within the FGF family. The Cβ-Cβ distance of 4.6 Å between Cys-83 and Cys-79, which is exposed and bonded to a water molecule, is sufficient for disulfide bond formation. However, no intramolecular or intermolecular disulfide bonds were evident.

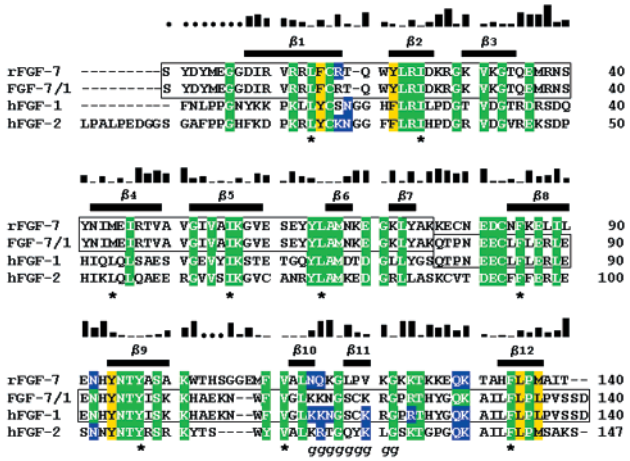

FIGURE 2: Sequence alignment and structural features. Sequences of rat (r) FGF-7 (SWISSPROT Q02195), chimeric rat FGF-7/human FGF-1 (FGF-7/1) and human (h) FGF-1 (A33665) and human (h) FGF-2 (P09038) were aligned. The β-strands of FGF-7 are indicated. Homologous domains between chimeric FGF-7/1 and FGF-7 and FGF-1 are boxed. Conserved residues in FGF-1, FGF-2, and FGF-7 are highlighted in green and yellow (phenylalanine/tyrosine and aspartate/glutamate were scored as conserved). H-patch residues are shown in yellow and heparin contact residues derived from cocrystals with FGF-1 and FGF-2 or by homology in FGF-7 are in blue. Residues in the G-box domain, which has been implicated in the specificity of FGF-7 for FGFR (*20*), are denoted by g. Conserved hydrophobic residues that form the inner core of FGF-7 are indicated by asterisk. Surface accessibility calculated by SURFACE of CCP4 of each FGF-7 residue is indicated by the histogram. Disordered residues are indicated by black dots.

Conserved Hydrophobic Patch and Homologous Heparin-Binding Domain. Comparison of the structures of FGF-7 and chimeric FGF-7/1 with those of FGF-1 and FGF-2 revealed the conservation among the four factors of a distinctive surface patch that is dominated by hydrophobic residues (H-patch) (Figure 2) and flanked by polar amino acids. The solvent-accessible area of the H-patch was calculated with the program SURFACE of CCP4 and a probe radius of 1.4 Å. In FGF-7, the five hydrophobic residues of the H-patch, Phe-16, Tyr-22, Tyr-94, Leu-135, and Met-137 are conserved among all FGF homologues and formed an area of 241 Å^2. Addition of residues Gln-35 and Asn-92 results in an area of 452 Å^2. The homologous hydrophobic H-patch residues (Tyr-25, Phe-32, Tyr-104, Leu-141, Met-143) and homologous residues Arg-45 and Asn-102 in FGF-2 have been implicated in receptor binding by mutagenesis (*33*). They dominate the interaction between immunoglobulin (Ig) module II in the crystal structure of a heparin-independent complex of FGFR1 and FGF-2 (*34*). The comparable areas in chimeric FGF-7/1 were 222 and 443 Å^2, respectively. Conservation of the H-patch is consistent with observations that FGF-1, FGF-2, and FGF-7 interact with a complex of heparin and Ig module II of FGFR1 and FGFR2 in absence of flanking structural domains (*35*−*37*).

By comparison to the structures of a complex of FGF-1 (*11*) and FGF-2 (*19*) with a heparin hexasaccharide, FGF-7 exhibits a homologous heparin-binding domain comprised of residues Arg-18, Asn-92, Asn-114, Gln-115, Val-120, Lys-124, Gln-129, Lys-130, and Thr-131 (Figures 2 and 3). The counterpart residues in the chimeric FGF-7/1 were Arg-18, Asn-92, Lys-112, Lys-113, Lys-118, Arg-119, Arg-122, Gln-127, and Lys-128.

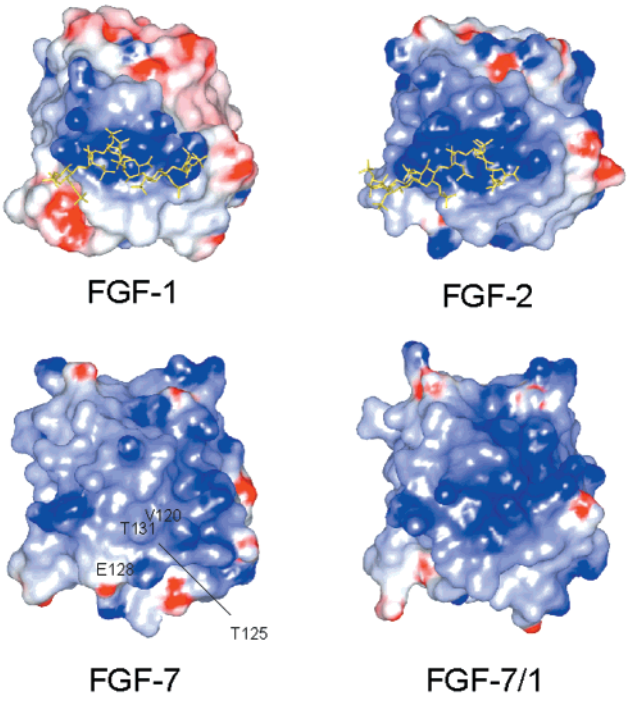

FIGURE 3: Comparison of the distribution of surface electrostatic potential of homologous HB domains among four FGF homologues. Charge potential less than −10 KT, neutral, and greater than 10 KT is displayed in red, white, and blue, respectively. The heparin hexasaccharide in the cocrystals of FGF-1 and FGF-2 is shown in yellow. The four molecules were superimposed and are rotated to the same orientation showing the HB domain. Superimposition of the atoms was performed with the program LSQKAB of CCP4. The PDB codes are 2AXM (*11*) and 1BFC (*19*) for FGF-1 and FGF-2, respectively. Specific residues that reduced the surface potential in FGF-7 are indicated. Surface charge distribution was calculated and displayed by the program GRASP and rendered by POV-Ray (*46*).

Unique Surface Charge Distribution of the HB Domain and Affinity for 3-O-Sulfated Heparin. In concert with FGF-7 overall, the Cα backbone of the homologous HB domain of the chimeric FGF-7/1 and FGF-7 was similar (rmsd < 1 Å) to FGF-1 and FGF-2. However, the side chains and distribution of surface charge surrounding the homologous domain on FGF-7 were dramatically different (Figure 3). Whereas the positive surface potential (blue) on FGF-1, FGF-2, and the FGF-7/1 chimera is concentrated, it is dispersed on the FGF-7 structure. The homologous area on FGF-7 to that on FGF-1 and FGF-2 with concentrated positive surface charge potential is disrupted and divided into two parts by residues Val-120, Thr-125, and Thr-131. Thr-125 is conserved among the three FGFs. Val-120 is a lysine, which contacts heparin, and Thr-131 is an alanine in FGF-1 and FGF-2. Loss of the charged lysine side chain by substitution of Val-120 in FGF-7 results in exposure of residues Thr-125 and Thr-131 and a cavity that separates the two areas of concentrated charge. Although the substitution of the heparin-contact residue lysine with valine results in a loss of charge, the rearrangement would cause no spatial conflict with a heparin chain that spans the two charge-dense areas. Negatively charged Glu-128, which is unique to FGF-7 and near the HB domain, might negatively impact the interaction of heparin. These observations are consistent with the different salt concentrations required to break the interaction between FGF-7 and

heparin relative to FGF-1 and FGF-2 (*32*) and suggest that the structural requirements within heparin may be different.

Interactions in the crystal structures of complexes of heparin oligosaccharides with FGF-1 (*11*) and FGF-2 (*19*) are consistent with the sulfation requirements suggested by experiment. 2-O-sulfation of heparin appears sufficient for FGF-2 binding, while FGF-1 requires both 2-O-sulfate and 6-O-sulfate (*38*, *39*). Attempts to cocrystallize FGF-7 or soak crystals of FGF-7 with the heparin hexasaccharide, which contained 2-O and 6-O, but no 3-O-sulfate, that cocrystallized with FGF-2 (*19*) yielded crystals identical to those described for FGF-7 alone. Therefore, we performed experiments to determine whether the simple heparin hexasaccharide interacted with FGF-7 at all. Stabilization and protection against protease is one function of the interaction of FGF and pericellular matrix heparan sulfate and therefore has been exploited to monitor the functional interaction of heparin oligosaccharides with FGF as well as a convenient affinity matrix for preparative scale proteolytic modification (*3*). The hexasaccharide at 250 ng/mL protected FGF-1 and FGF-2 at 44 and 69% the efficacy of crude heparin at 100 ng/mL, respectively. However, the same amount of hexasaccharide at a molar ratio of 1200 oligosaccharide/FGF-7 failed to protect FGF-7 at all (Figure 4). However, at 250 ng/mL a recent structurally defined decasaccharide (AT10) derived from heparin with heparinase I (*29*) at a molar ratio of 700 was able to protect FGF-7 at 33% the efficacy of 100 ng/mL heparin. A partially defined tetradecasaccharide (AT-14) derived by the same method (*28*) was about twice as effective as AT10 at a molar ratio of 500. In addition to the increased length, both AT10 and AT14 are distinguished from the hexasaccharide by the presence of a 3-O-sulfate on N-sulfated, 6-O sulfated glucosamine (*28*, *29*, *30*). The 3-O-sulfate has been unequivocally established on an N-sulfated, 6-O sulfated glucosamine at the reducing terminus of AT10. Although reduced in magnitude relative to heparin and a complete anticoagulant pentasaccharide with α-L-IdoAp2S(1→4)-α-D-GlcNpS3S6S disaccharide on the reducing side of the glucosamine residue containing the 3-O-sulfate, the partial antithrombin-binding site is sufficient to impart a low, but detectable affinity for antithrombin and anti-factor Xa amydolytic activity (*30*). The hexasaccharide is devoid of both properties. These results suggest that the failure of the hexasaccharide to cocrystallize with FGF-7 likely

reflects a lack of sufficient structural properties to interact with the unique HB domain. The disruption and dispersion of the basic charge density, which differentiates the FGF-7 HB domain from that of FGF-1 and FGF-2, is consistent with an additional requirement for either 3-O-sulfated residues or increased length or both for the FGF-7-binding motif within heparin or heparan sulfate relative to FGF-1 and FGF-2.

To further dissect 3-O sulfation from length, we compared the activity of counterpart 10-mer and 14-mer oligosaccharides prepared from heparin by the same method as AT10 and AT14, but which exhibited no anticoagulant activity and which did not even show weak affinity for antithrombin (Figure 5). The ability of the 10-mer and 14-mer to protect FGF-7 was 44 and 30% that of AT10 and AT14, respectively. This increased efficacy in the oligosaccharides of heparin differing by only a 3-O-sulfate strongly implicates

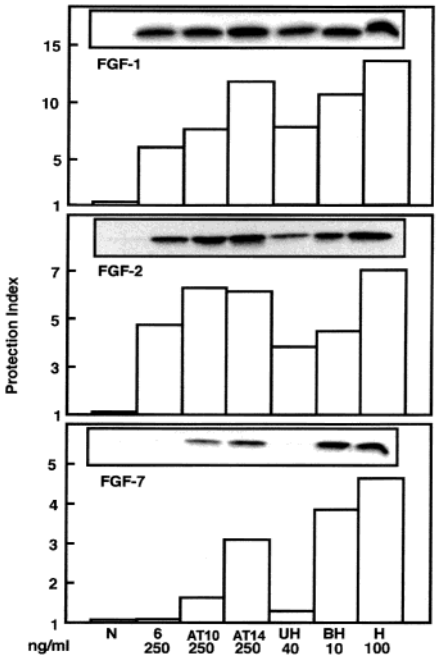

	N	6	AT10	AT14	UH	BH	H
cpm	4,392	4,880	7,832	11,624	5,508	16,632	18,264
Index	-	1.1	1.8	2.6	1.3	3.8	4.2

FIGURE 4: Protection of FGF-7 against protease requires heparin with properties different from FGF-1 and FGF-2. The heparin oligosaccharides and fractionated heparin were added to FGF-7 during incubation with Pronase as described in Experimental Procedures. The single indicated autoradiographic band of [^{125}I]-FGF which was identical in apparent molecular weight to the untreated material was excised and counted by liquid scintillation. The protection index was calculated by division of the amount of FGF remaining in the presence of heparin after protease treatment divided by the amount of FGF-1 (1800 cpm), FGF-2 (11 000 cpm) or FGF-7 (4400 cpm) remaining in absence of additive. Input was 36 800, 109 700, and 51 200 cpm for FGF-1, FGF-2, and FGF-7, respectively. Excised band count was 24 600, 79 000, and 21 000 cpm for FGF-1, FGF-2, and FGF-7, respectively, in the presence of 100 ng/mL heparin. In the bottom panel, the amount of TCA precipitable FGF-7 (input 34 300 cpm) remaining after the treatment in the presence of the same heparin fractions at the same concentrations was counted from an independent experiment. N = nothing added, 6, AT10, AT14 = 6-mer, AT 10-mer, and AT 14-mer oligosaccharides added, UH = heparin not binding ATIII added, BH = heparin binding ATIII added, H = unfractionated heparin added.

the 3-O-sulfate and the partial antithrombin-binding site in the interaction. The position of the 3-O-sulfate-containing glucosamine residue in AT14 is not yet proven. However, it was generated by the same method (by heparinase I cleavage) and exhibited a similar level of anti-factor Xa activity to AT10. Therefore, it is predicted that the 3-O-sulfate may also reside at the reducing end of AT14 giving a similar partial antithrombin-III-binding site to AT10. The approximately 1.5-fold increased effectiveness of AT14 over AT10 in protection of FGF-7 suggests a contribution of the increased length of this oligosaccharide. It is also noteworthy that, although the efficacy of the 10-mer and 14-mer, devoid of 3-O-sulfate, is reduced relative to AT10 and AT14 counterparts, the 14-mer detectably protects FGF-7 better than the 10-mer or 6-mer at the same or higher concentra-

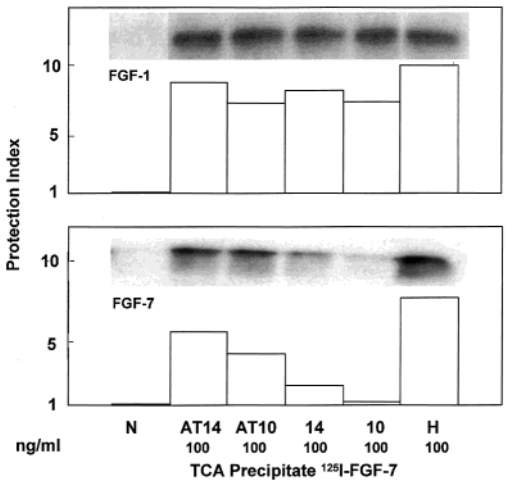

	N	AT14	AT10	14	10	H
cpm	3224	17290	13110	7572	3898	24548
Index	-	5.4	4.1	2.3	1.3	7.6

FIGURE 5: Comparison of a heparin decasaccharide and tetradecasaccharide differing by a 3-O-sulfate on protection of FGF-7. Ability to protect FGF-1 and FGF-7 against Pronase was determined as described in Figure 4. AT14 and AT10 indicate the tetradecasaccharide and decasaccharide, respectively, which exhibit a 3-O-sulfate and 14 and 10 indicated the same oligosaccharides that do not. H = heparin. Input was 28 450 and 38 500 cpm for FGF-1 and FGF-7, respectively. Excised band count was 20 750 and 25 590 cpm for FGF-1 and FGF-7 in the presence of 100 ng/mL heparin, and 1920 and 3640 cpm for FGF-1 and FGF-7 in the absence of 100 ng/mL heparin. The input for TCA precipitable FGF-7 was 41 600 cpm.

tions. This suggests a role of both 3-O sulfation and increased length in interaction with the unique HB-domain of FGF-7 relative to FGF-1 and FGF-2. Neither AT10 nor AT14 at molar ratios of 700 and 500 to FGF-7 was equal to the protective effect of 100 ng/mL of crude heparin, a molar ratio of heparin to FGF-7 of about 40 if the manufacturer's estimate of 17−19 kDa is assumed. This level of heparin is the minimum that resulted in maximum protection of FGF-7 from proteolysis.

We also fractionated crude heparin using antithrombin affinity chromatography and then tested the bound (BH) and unretained (UH) fractions for ability to protect FGF-7. The antithrombin-bound heparin was at least 3.5 times more effective at one-fourth the concentration than the unbound fraction (UH) for protection of FGF-7 against protease (Figure 4). After repeated chromatography that removed detectable anti-factor Xa activity, the unbound fraction failed to protect FGF-7 at concentrations up to 10 μg/mL after which aggregation and precipitation of FGF-7 occurred (results not shown). In contrast, the unretained fraction was 80−90% as effective as the bound fraction for protection of FGF-1 and FGF-2. Assuming that the average molecular weights of the bound and unbound fractions are similar, the results indicate that a ratio as low as 4 mol of the antithrombin-binding heparin to 1 mol FGF-7 protects it against protease. Since it is conceivable that the antithrombin affinity column may enrich longer chains of heparin because they have higher probability of containing one or more rare motifs containing 3-O-sulfates that interact with FGF-7, the molar ratio may be an overestimate. These results strongly

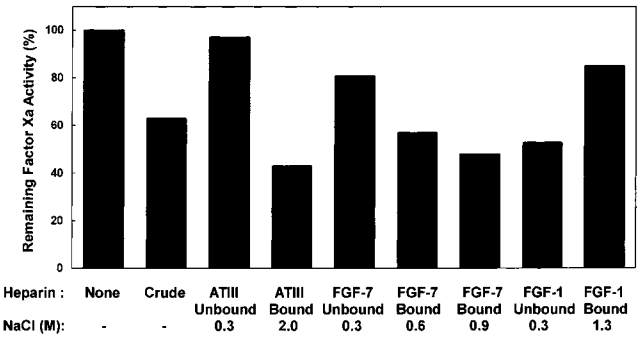

FIGURE 6: Specificity of FGF-7 for the crude heparin fraction with anti-factor Xa activity. Antithrombin III (170 nM) was incubated with Factor Xa (5 nM) in the presence of 100 ng/mL of the indicated fractions of heparin generated by FGF-7, FGF-1, or antithrombin affinity chromatography. The remaining Factor Xa activity was determined as absorbance unit with a chromogenic substrate at A_{405} as described in the Experimental Procedures and was expressed as a percentage of Factor Xa activity in the presence of antithrombin III devoid of heparin. Data points represent the mean of duplicates from a single experiment with a single preparation of affinity-purified heparin. The data are representative of three independent preparations by affinity chromatography.

suggest a role of the high affinity antithrombin-binding motif in heparin for functional interaction with the unique HB domain of FGF-7. The high molar ratio of 500−700 AT10 and AT14 required to protect FGF-7 relative to that of the antithrombin-bound fraction of crude heparin is consistent with absence of the complete antithrombin-binding sequence and insufficient length of the oligosaccharides.

Finally, we determined whether immobilized FGF-7 selectively enriched the antithrombin-binding motif from crude heparin. Previously, we showed that although GST fused at the N-terminus of FGF-7 interferes with the binding to the FGFR−heparin complex, it does not interfere with the FGR-independent specific interaction of heparin (*20*). This property was exploited in large-scale preparative procedures to remove the GST fusion partner by trypsin treatment without effect on FGF-7. Crude heparin was applied at 0.3 M NaCl to GST-FGF-7 immobilized through salt-resistant binding to GSH−Sepharose, and, after extensive washing, fractions were then eluted at 0.6 and 0.9 M. FGF-7-bound heparin at 100 ng/mL, which eluted at 0.6 and 0.9 M NaCl, exhibited anti-factor Xa activity that was 75 and 90%, respectively, of that exhibited by the same amount of the heparin fraction retained by ATIII immobilized on ConA-Sepharose (Figure 6). Surprisingly, immobilized GST-FGF-1 appeared to reject heparin displaying the anti-factor Xa activity. The FGF-1-bound fraction exhibited a 60% reduction in activity relative to unfractionated heparin while the unbound fraction exhibited anti-factor Xa activity which was 82% of the activity of fractions retained by antithrombin columns (Figure 6). These results confirm that the unique HB domain of FGF-7 selects for the antithrombin-binding motif in heparin that distinguishes it from FGF-1 and FGF-2. Further, a combination of both recombinant GST-FGF-1 and GST-FGF-7 affinity chromatography may be of utility in the extraction of anticoagulant heparin from crude stocks.

Structural Basis of Requirement of the Unique FGF-7 HB Domain for a Longer Heparin Sequence Motif Containing 3-O-Sulfate. We constructed a model complex of FGF-7 with the heparin hexasaccharide structure revealed in the cocrystals of FGF-1 and FGF-2 as shown in Figure 7. The model

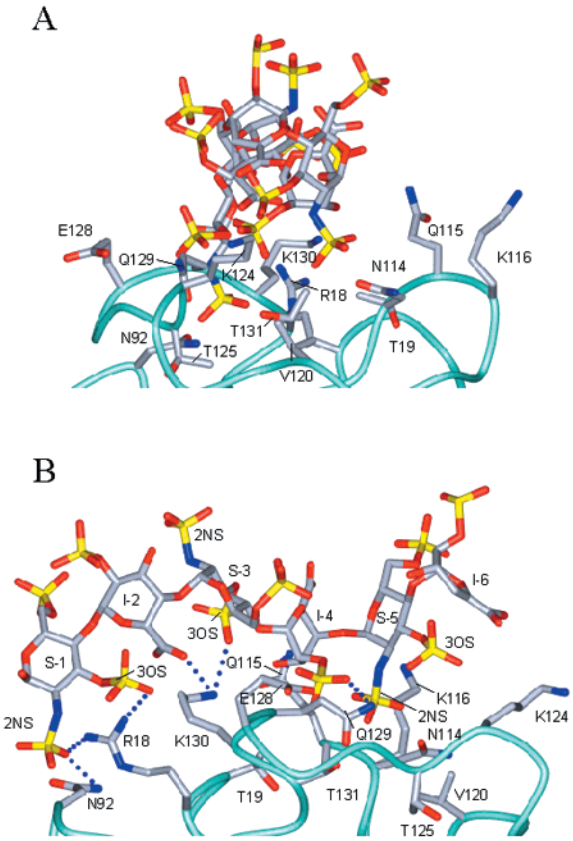

FIGURE 7: Homology models of heparin hexasaccharides bound to the HB domain of FGF-7. (A) Heparin hexasaccharide devoid of 3-O-sulfate described in crystal structures for FGF-1 and FGF-2. The model was built using program O (*25*) and Bobscript (*47*) as described in the text and rendered by POV-Ray (46). The view is from the nonreducing end of the hexasaccharide with the reducing end going into the plane of the paper. (B) Heparin hexasaccharide with 3-O-sulfates at three possible positions. The single illustration should be viewed as four different models, one with no 3-O sulfation and three variants with a single 3-O-sulfate at the positions denoted "3OS" as described in the text. Dashed lines show potential salt bridges. The view is the model in panel A rotated about 90° to the right. S = glucosamine; I = iduronic acid; 2NS = 2-N-sulfate.

was based on (1) the assumption that the backbone of the FGF-7 heparin-binding site is homologous to that of FGF-1 and FGF-2; (2) maintenance of the torsion angles of the heparin hexasaccharide within the calculated allowed region for the heparin polymer and close to those derived from NMR data (*40*); and (3) maintenance of three contacts (observed in both FGF-1 and FGF-2 structures) between the hexasaccharide and the common backbone of all four FGFs. The common contacts were those between 2-N-sulfate of residue 5 of the heparin hexasaccharide with the backbone N of Gln-115 and the 2-O-sulfate of residue 4 with the backbone N of Lys-130 and Thr-131. The model showed that Lys-116 and Val-120 in FGF-7, which are the counterparts of heparin-contact residues in FGF-1 (Figure 2), could not participate in the binding of heparin (Figure 7A). Lys-116 replaces the heparin-binding Asn-114 in FGF-1. Val-120 replaces the heparin-binding Lys-118 in FGF-1 and Lys-126 in FGF-2. The loop between β strand 1 and 2 in FGF-7 is one residue shorter than that of FGF-1 and FGF-2. As a consequence, the FGF-7 counterpart, Thr-19, of the heparin-binding asparagine in FGF-1 (Asn-18) and FGF-2 (Asn-28) was also too far from heparin to form hydrogen bonds with the 2-N-sulfate of GlcN residue 3 and the 3-OH of IdoA residue 2. These contacts were observed in the cocrystals of FGF-1 and FGF-2.

In Figure 7B, three single 3-O-sulfated variants in one model were generated by manually adding a 3-O-sulfate group to each of the three glucosamine-N-sulfate residues of the heparin hexasaccharide. Assuming that addition of the 3-O groups does not cause significant conformational change in either the oligosaccharide or FGF-7, new theoretical charge interactions were noted in each of the three models as follows: model 1 with the single glucosamine-N-sulfate-3-O-sulfate at position 1 (S-1), which would require GlcNAc-(6-O-sulfate)-GlcA at the nonreducing end to fit the antithrombin binding motif, exhibited the most elaborate network, with both the 2-N-sulfate and 3-O-sulfate participating in salt bridges with Arg-18, as well as a 2-N-sulfate interaction with Asn-92 (Figure 7B). If the classical high-affinity antithrombin-binding motif was maintained, however, this would be at the expense of loss of the interaction with 6-COO^- of IdoA (I-2), which would be replaced with GlcA. In model 2, if a single 3-O-sulfate in glucosamine-N-sulfate-3-O-sulfate were at position 3 (S-3), Lys-130 can form a new salt bridge with the 3-O-sulfate. Again, if the antithrombin motif were maintained by substitution of IdoA (I-4) with GlcA, the hydrogen bond with Q129 would also be lost. In the third 3-O-sulfated variant of the model, a 3-O-sulfate at position 5 made no new contacts. The described models were limited to the hexasaccharide backbone for which the structure bound to FGF is known. It was apparent from separate modeling exercises that an increase in length of the hexasaccharide beginning at residue IdoA-6 with heparin disaccharide repeats would give rise to additional charge interactions with FGF-7 beginning at Lys-124. Although this modeling exercise involved the stepwise addition of a single 3-O-sulfate at different monosaccharide residues within the hexasaccharide and was discussed in context of preservation of the classic anticoagulant motif, it is conceivable that rare FGF-7- and FGFR-specific motifs overlap with, but are not identical to, structural elements in the classic optimum anticoagulant pentasaccharide motif.

In summary, the model suggests losses of favorable interactions with the FGF-1/FGF-2-binding hexasaccharide within the homologous FGF-7 HB domain that were present within the HB domain of FGF-1 and FGF-2. FGF-7 residues Thr-19 and Val-120, which do not participate in the binding of heparin in the model, together with Thr-125 and Thr-131, occupy the area in FGF-7 that is occupied by heparin-contact residues Asn-18 and Ala-129 in FGF-1. These residues have major impact on disruption and reduction in the positive charge potential across the homologous FGF-7 HB domain. These differences may generate a requirement for a unique pattern of sulfation including 3-O and increased length of the oligosaccharide.

The model presented in Figure 7 illustrates the orientation of the hexasaccharide in respect to polarity of the reducing and nonreducing ends relative to the homologous HB-domain in FGF-7 that has been reported for both FGF-1 and FGF-2 (*11*, *19*). The reverse orientation to that shown has also been described for the independent interaction of a heparin dodecasaccharide with FGF-1 (*11*). Two fundamentally different crystal structures in respect to subunit stoichiometry and orientation of heparin in an oligomeric complex of FGF,

FGFR, and the same heparin dodecasaccharide have been recently reported (*41*, *42*). The reason for the difference is likely to be a combination of nonphysiological ionic conditions and an artificial heparin oligosaccharide devoid of anticoagulant activity. One or more elements of the anticoagulant motif are required for the specific interaction of heparin/heparan sulfate with the FGFR ectodomain under physiological conditions in absence of FGF (*37*, *43*). The common feature of both structures is the orientation and interaction interface of the oligosaccharide which reacts concurrently with both an FGF and FGFR in ternary complex similar to that which we have proposed previously (*2*). The polarity of the oligosaccharide in respect to FGF in the ternary interaction is opposite to that shown in the model in Figure 7. One structure (PDB code 1FQ9) (*41*) with 2 FGF:2 oligosaccharide:2 FGFR stoichiometry is symmetric with two similar ternary interactions of FGF (*2*, *37*), oligosaccharide, and FGFR. The other structure (PDB code 1EOO) with 2 FGF:1 oligosaccharide:2 FGFR is asymmetric with one ternary interaction in common with (PDB code 1FQ9), but with the other end of the single oligosaccharide in contact with only the HB-domain of another FGF bound to another FGFR (*42*). The latter interaction that is FGFR-independent shows the opposite orientation of the oligosaccharide in respect to FGF than that observed in the ternary complex and is the same orientation as that shown in the FGFR-independent interaction of heparin with FGF-7 in Figure 7. The fact that the orientation of heparin oligosaccharide is common in the ternary complex in both crystal structures suggests that the common orientation may be preferred for the concurrent interaction of a heparin or heparan sulfate oligosaccharide motif with both FGF and FGFR which is also much more stringent in respect to oligosaccharide length and composition (*11*, *19*). The orientation captured in one of the dimers in 1E00 and shown in Figure 7 may be the preferred orientation for the independent interaction with FGF. Whether a single orientation or either underlies the interaction of FGF-7 and specific oligosaccharide in the protease protection assay awaits determination of structure of the specific FGF-7-oligosaccharide complex.

Conclusions. FGF-7 exhibits restricted expression and specificity for receptor, which contributes to a directional paracrine signaling system from the stromal to epithelial compartment in many parenchymal tissues (*14*−*16*, *44*). Subversion of the system results in loss of instructive signals between compartments (*2*, *15*, *16*, *44*). Despite the specificity of FGF-7 for complexes of heparan sulfate-FGFR2IIIb in epithelial cells, the layout of the Cα backbone and structural domains of FGF-7 is remarkably similar to FGF-1, FGF-2, and the FGF-7/FGF-1 chimera. Unless dramatic conformational change in the backbone occurs in complex with heparan sulfate, the receptor kinase, or in the ternary complex with both, the specificity must lie in the composition and orientation of side-chain residues. To date, extensive conformational change of the Cα backbone of FGF-1 or FGF-2 does not occur in complex with heparin (*11*, *17*−*19*) or in the heparin-independent complex of FGF-2 with FGFR1 (*34*). The notable difference caused by unique side-chain residues of FGF-7 is a different surface structure of the homologous FGF-7 HB domain that correlates with additional demands on the structure of the interactive heparin/heparan sulfate. These differences include residues within the glycine-box (G-box) that have been identified as a major determinant of the specificity of FGF-7 for FGFR2IIIb in epithelial cells (*20*, Figure 2).

Our results suggest for the first time a role of structural elements, in particular 3-O sulfation, that overlaps with the antithrombin-binding motif of heparan sulfate chains in the FGFR-independent interaction with FGF. The FGFR-independent interaction of heparan sulfate with FGFs has been proposed to promote oligomerization (*8*, *9*, *11*) and sequester and protect FGF within the peri-cellular matrix (*3*, *4*, *5*, *32*). Restrictions on the structure of heparan sulfate that interacts with FGF-7 may restrict its half-life, localization and trafficking in the peri-cellular environment relative to FGF-1 and FGF-2. Peri-cellular matrix binding sites expressed by prostate epithelial cells for FGF-7 are a fraction of the binding sites for a homologue, FGF-10, which is also expressed in the stroma and also acts on epithelial cell FGFR2IIIb (*32*).

Structural elements enriched in the anticoagulant motif are also required for heparin or cellular heparan sulfate to form a specific binary complex with the FGFR ectodomain under physiological conditions that is competent to bind FGF-1, FGF-2 (*42*), FGF-7, and FGF-10 and most likely all FGF ligands. A single heparan sulfate oligosaccharide with combined properties sufficient to concurrently bind FGF-7 and FGFR2IIIb (*31*, *43*, *45*) into a ternary complex may be rare and the main determinant in the specificity of FGF-7 signaling.

REFERENCES

1. Martin, G. R. (1998) *Genes Dev. 12*, 1571−1586.
2. McKeehan, W. L., Wang, F., and Kan, M. (1998) *Prog. Nucleic Acid Res. Mol. Biol. 59*, 135−176.
3. Luo, Y., Gabriel, J. L., Wang, F., Zhan, X., Maciag, T., Kan, M., and McKeehan, W. L. (1996) *J. Biol. Chem. 271*, 26876−26883.
4. Vlodavsky, I., Miao, H. Q., Medalion, B., Danagher, P., and Ron, D. (1996) *Cancer Metastasis Rev. 15*, 177−186.
5. Friedl, A., Chang, Z., Tierney, A., and Rapraeger, A. C. (1997) *Am. J. Pathol. 150*, 1443−1455.
6. Kato, M., Wang, H., Kainulainen, V., Fitzgerald, M. L., Ledbetter, S., Ornitz, D. M., and Bernfield, M. (1998) *Nat. Med. 4*, 691−697.
7. Ornitz, D. M., Herr, A. B., Nilsson, M., Westman, J., Svahn, C. M., and Waksman, G. (1995) *Science 268*, 432−436.
8. Herr, A. B., Ornitz, D. M., Sasisekharan, R., Venkataraman, G., and Waksman, G. (1997) *J. Biol. Chem. 272*, 16382−16389.
9. Moy, F. J., Safran, M., Seddon, A. P., Kitchen, D., Bohlen, P., Aviezer, D., Yayon, A., and Powers, R. (1997) *Biochemistry 36*, 4782−4791.
10. Waksman, G., and Herr, A. B. (1998) *Nat. Struct. Biol. 5*, 527−530.
11. DiGabriele, A. D., Lax, I., Chen, D. I., Svahn, C. M., Jaye, M., Schlessinger, J., and Hendrickson, W. A. (1998) *Nature 393*, 812−817.
12. Kan, M., Wang, F., Xu, J., Crabb, J. W., Hou, J., and McKeehan, W. L. (1993) *Science 259*, 1918−1921.
13. Kan, M., Wang, F., To, B., Gabriel, J. L., and McKeehan, W. L. (1996) *J. Biol. Chem. 271*, 26143−26148.
14. Finch, P. W., Rubin, J. S., Miki, T., Ron, D., and Aaronson, S. A. (1989) *Science 245*, 752−755.
15. Yan, G., Fukabori, Y., McBride, G., Nikolaropolous, S., and McKeehan, W. L. (1993) *Mol. Cell. Biol. 13*, 4513−4522.
16. Feng, S., Wang, F., Matsubara, A., Kan, M., and McKeehan, W. L. (1997) *Cancer Res. 57*, 5369−5378.

17. Zhu, X., Komiya, H., Chirino, A., Faham, S., Fox G. M., Arakawa, T., Hsu, B. T., and Rees, D. C. (1991) *Science 251*, 90−93.
18. Eriksson, A. E., Cousens, L. S., Weaver, L. H., and Matthews, B. W. (1991) *Proc. Natl. Acad. Sci. U.S.A. 88*, 3441−3445.
19. Faham, S., Hileman, R. E., Fromm, J. R., Linhardt, R. J., and Rees, D. C. (1996) *Science 271*, 1116−1120.
20. Luo, Y., Lu, W., Mohamedali, K. A., Jang, J.-H., Jones, R. B., Gabriel, J. L., Kan, M., and McKeehan, W. L. (1998) *Biochemistry 37*, 16506−16515.
21. Hendrickson, W. A., Horton, J. R., and LeMaster, D. M. (1990) *EMBO J. 9*, 1665−1672.
22. Otwinowski, Z., and Minor, W. (1997) *Methods Enzymol. 276*, 307−326.
23. Ramakrishnan, V., and Biou, V. (1997) *Methods Enzymol. 276*, 538−557.
24. Terwilliger, T. C. (1997) *Methods Enzymol. 276*, 530−537.
25. Jones, T. A., Zou, J. Y., Cowan, S. W., and Kjeldgaard. (1991) *Acta Crystallogr., Sect. A 47*, 110−119.
26. Brünger, A. T. (1992) in *X-PLOR Version 3.1: A System for X-ray Crystallography and NMR*, pp 1−382, Yale University Press, New Haven.
27. Navaza, J. (1994) *Acta Crystallogr., Sect. A 50*, 157−163.
28. Toida, T., Hileman, R. E., Smith, A. E., Vlahova, P. I., and Linhardt, R. J. (1996) *J. Biol. Chem. 271*, 32040−32047.
29. Shriver, Z., Raman, R., Venkataraman, G., Drummond, K., Turnbull, J., Toida, T., Linhardt, R., Biemann, K., and Sasisekharan, R. (2000) *Proc. Natl. Acad. Sci. U.S.A. 97*, 10359−10364.
30. Shriver, Z., Sundaram, M., Venkataraman, G., Fareed J., Linhardt, R., Biemann, K., and Sasisekharan, R. (2000) *Proc. Natl. Acad. Sci. U.S.A. 97*, 10365−10370.
31. Kan, M., Wu, X., Wang, F., and McKeehan, W. L. (1999) *J. Biol. Chem. 274*, 15947−15952.
32. Lu, W., Luo, Y., Kan, M., and McKeehan, W. L. (1999) *J. Biol. Chem. 274*, 12827−12834.
33. Springer, B. A., Pantoliano, M. W., Barbera, F. A., Gunyuzlu, P. L., Thompson, L. D., Herblin, W. F., Rosenfeld, S. A., and Book, G. W. (1994) *J. Biol. Chem. 269*, 26879−26884.
34. Plotnikov, A. N., Schlessinger, J., Hubbard, S. R., and Mohammadi, M. (1999) *Cell 98*, 641−650.
35. Wang, F., Kan, M., Xu, J., Yan, G., and McKeehan, W. L. (1995) *J. Biol. Chem. 270*, 10222−10230.
36. Wang, F., Lu, W., McKeehan, K., Mohamedali, K., Gabriel, J. L., Kan, M., and McKeehan, W. L. (1999) *Biochemistry 38*, 160−171.
37. Uematsu, F., Kan, M., Wang, F., Jang, J.-H., Luo, Y., and McKeehan, W. L. (2000) *Biochem. Biophys. Res. Commun. 272* (3), 830−836.
38. Guimond, S., Maccarana, M., Olwin, B. B., Lindahl, U., and Rapraeger, A. C. (1993) *J. Biol. Chem. 268*, 23906−23914.
39. Ishihara, M., Kariya, Y., Kikuchi, H., Minamisawa, T., and Yoshida, K. (1997) *J. Biochem. (Tokyo) 121*, 345−349.
40. Mikhailov, D., Linhardt, R. J., and Mayo, K. H. (1997) *Biochem. J. 328*, 51−61.
41. Schlessinger, J., Plotnikov, A. N., Ibrahimi, O. A., Eliseenkova, A. V., Yeh, B. K., Yayon, A., Linhardt, R. J., and Mohammadi, M. (2000) *Mol. Cell. 6*, 743−750.
42. Pellegrini, L., Burke, D. F., von Delft, F., Mulloy, B., and Blundell, T. L. (2000) *Nature 407*, 1029−1034.
43. McKeehan, W. L., Wu, X., and Kan, M. (1999) *J. Biol. Chem. 274*, 21511−21514.
44. Matsubara, A., Kan, M., Feng, S., and McKeehan, W. L. (1998) *Cancer Res. 58*, 1509−1514.
45. Wu, X., Kan, M., Wang, F., Jin, C., Yu, C., and McKeehan, W. L. (2001) *Cancer Res. 61*, 5295−5302.
46. POV-ray: the persistence of vision ray tracer (1998) (http://www.povray.org/).
47. Esnouf, B. M. (1997) *J. Mol. Graphics 15*, 133−138.

BI011000U